Preparation and electrochemical characterization of ionic-conducting lithium lanthanum titanate oxide/polyacrylonitrile submicron composite fiber-based lithium-ion battery separators

Yinzheng Liang [a,b], Liwen Ji [b], Bingkun Guo [b], Zhan Lin [b], Yingfang Yao [b], Ying Li [b], Mataz Alcoutlabi [b], Yiping Qiu [a], Xiangwu Zhang [b,*]

[a] Department of Textile Materials Science and Product Design, College of Textile, Donghua University, Shanghai, 201620, China
[b] Fiber and Polymer Science Program, Department of Textile Engineering, Chemistry and Science, North Carolina State University, Raleigh, NC, 27695-8301, USA

ARTICLE INFO

ABSTRACT

Lithium lanthanum titanate oxide (LLTO)/polyacrylonitrile (PAN) submicron composite fiber-based membranes were prepared by electrospinning dispersions of LLTO ceramic particles in PAN solutions. These ionic-conducting LLTO/PAN composite fiber-based membranes can be directly used as lithium-ion battery separators due to their unique porous structure. Ionic conductivities were evaluated after soaking the electrospun LLTO/PAN composite fiber-based membranes in a liquid electrolyte, 1 M lithium hexafluorophosphate (LiPF$_6$) in ethylene carbonate (EC)/ethyl methyl carbonate (EMC) (1:1 vol). It was found that, among membranes with various LLTO contents, 15 wt.% LLTO/PAN composite fiber-based membranes provided the highest ionic conductivity, 1.95×10^{-3} S cm^{-1}. Compared with pure PAN fiber membranes, LLTO/PAN composite fiber-based membranes had greater liquid electrolyte uptake, higher electrochemical stability window, and lower interfacial resistance with lithium. In addition, lithium//1 M LiPF$_6$/EC/EMC//lithium iron phosphate cells containing LLTO/PAN composite fiber-based membranes as the separator exhibited high discharge specific capacity of 162 mAh g^{-1} and good cycling performance at 0.2 C rate at room temperature.

1. Introduction

High energy demands have accelerated emergent efforts to develop high-performance rechargeable lithium-ion batteries (LIBs) due to their high energy and power densities, long cycle life, and broad applications in various fields, such as mobile telephone, portable computer, camcorder and hybrid electric vehicles [1–4]. In the LIB system, the separator plays an important role by regulating cell kinetics, preventing electronic contact between electrodes, and maintaining liquid electrolyte in cells [5–8]. Currently, most LIBs use conventional microporous polyolefin membranes as the separator. Polyolefin microporous membranes have good chemical stability, suitable thickness, and reasonable mechanical strength, but they have low thermal stability, low porosity, and poor wettability with polar liquid electrolyte, which lead to high cell resistance, reduced energy density, and low rate capability of rechargeable LIBs [5–10].

Research indicates that nonwoven separators have the potential to replace microporous polyolefin membranes to decrease the cost and increase both the porosity and air permeability [8]. However, most traditional nonwoven materials have large pore size and can lead to safety concerns when they are directly used as LIB separators. More recently, electrospinning technology has been developed to fabricate novel nano or submicron fiber-based nonwoven membranes, which have small pore size and large porosity, and can be directly used as separators in rechargeable LIBs [8,9–14]. These electrospun polymer membranes enable high-rate charge/discharge of LIBs because of their high porosity and desirable pathways for ion transport.

In this paper, ionic-conducting ceramic particles were introduced into electrospun polyacrylonitrile (PAN) fibers to provide the opportunity to obtain porous nonwoven membranes that not only have the basic functions of battery separators, but also can conduct lithium ions, which can significantly improve the battery kinetics. Perovskite-type lithium lanthanum titanate, Li$_{3x}$La$_{2/3-x}$TiO$_3$ (abbreviated as LLTO), was used as the ionic-conducting ceramic due to its high bulk lithium-ion conductivity of about 10^{-3} S cm^{-1} at room temperature [15–21]. Results show that the introduction of LLTO into composite fiber membranes can combine the advantageous properties of both components and lead to new composite separators that have large liquid electrolyte uptake, high ionic conductivity, good electrochemical stability, improved safety,

* Corresponding author. Tel.: +1 919 515 6547; fax: +1 919 515 6532.
E-mail address: xiangwu_zhang@ncsu.edu (X. Zhang).

and reduced electrode–electrolyte interface resistance. As a result, the new LLTO/PAN composite fiber-based membranes can provide ideal structure and properties for separating electrodes, supporting electrolytes, and transferring lithium ions, and lithium-ion cells using these membrane separators can achieve good battery performance, such as large capacity, good cycleability, high-rate capability, and enhanced safety.

2. Experimental

2.1. Chemicals

$LiNO_3$, $La(NO_3)_3 \cdot 6H_2O$, and $Ti(OC_4H_9)_4$ were used as precursors for LLTO particles. PAN and N,N-dimethylformamide (DMF) were used as the polymer and solvent, respectively, for the electrospinning of composite fiber membranes. All these reagents were purchased from Aldrich and were used without further purification.

2.2. LLTO particle preparation

Lithium-ion conducting LLTO particles were prepared by the sol–gel method starting from stoichiometry amount (0.35:0.55:1.00) of $LiNO_3$, $La(NO_3)_3 \cdot 6H_2O$, and $Ti(OC_4H_9)_4$ [15–21]. The aqueous solution of precursors was kept at 80 °C for 30 min with magnetic stirring to get a homogeneous gel, followed by drying at 150 °C. The dried mixture was pyrolyzed at 350 °C for 4 h and then calcined at 900 °C for 2 h with the heating rate of 5 °C min^{-1}. The calcined product was ground in an agate mortar and then sieved through a #325 mesh for further use.

2.3. Composite fiber preparation

LLTO/PAN composite fiber-based membranes were prepared by electrospinning DMF solutions of 8 wt. % PAN containing different amount of LLTO particles (0, 5, 10, and 15 wt.%), which were prepared at 70 °C with mechanical stirring for at least 24 h. During electrospinning, a variable high-voltage power supply (Gamma ES40P-20W/DAM) was used to provide a high voltage of around 18 kV. The flow rate and needle-to-collector distance used were 0.5 ml h^{-1} and 18 cm, respectively. Electrospun fibers were accumulated on the aluminum foil placed on the grounded collector to form porous nonwoven membranes. The resultant fiber-based porous membranes were dried in vacuum at 60 °C for 12 h before further use.

2.4. Structure characterization

The structure of LLTO particles was examined using scanning electron microscopy (JEOL 6400F Field Emission SEM at 5 kV) and wide-angle X-ray diffraction (WAXD, Philips X'Pert PRO MRD HR X-Ray Diffraction System, Cu kα, λ = 1.5405 Å). The morphology and diameter of LLTO/PAN composite fibers were evaluated using the same SEM. The average fiber diameters were calculated based on 100 randomly selected fibers in SEM images using Revolution v1.6.0 software.

2.5. Liquid electrolyte uptake

Liquid electrolyte uptakes of electrospun LLTO/PAN composite fiber-based membranes were measured by immersing weighed composite fiber membranes in the liquid electrolyte of 1 M lithium hexafluorophosphate ($LiPF_6$) dissolved in 1/1 (V/V) ethylene carbonate (EC)/ethyl methyl carbonate (EMC) (Ferro Corp.) for 2 h until an equilibrium was achieved in an argon-filled glove box. Liquid electrolyte-soaked LLTO/PAN composite fiber-based membranes were weighed quickly after removing the excrescent surface solution using wipes. The electrolyte uptake (EU) was calculated by the equation: EU (%) = $(W_f - W_0)/W_0 \times 100$, where W_f and W_0 are the weights of the electrolyte-soaked membranes and dry membranes, respectively.

2.6. Performance evaluation

The ionic conductivities of liquid electrolyte-soaked LLTO/PAN composite fiber-based membranes were measured by electrochemical impedance spectroscopy (EIS) using Reference 600 Potentiostat/Galvanostat/ZRA (GAMRY). During the measurements, the liquid electrolyte-soaked LLTO/PAN composite fiber-based membranes were sandwiched between two symmetrical stainless-steel plate electrodes and sealed. The impedance measurements were performed at amplitude of 10 mV over a frequency range of 1000 kHz to 1 Hz at a temperature range between 25 and 90 °C. The high-frequency intercept of the Nyquist plot on the real-axis gives the resistance R_b of liquid electrolyte-soaked LLTO/PAN composite fiber-based membranes. The ionic conductivities (σ) were calculated from the equation $\sigma = d/R_b \cdot S$, where d is the membrane thickness, and S the membrane cross-sectional area.

The electrochemical stability windows of liquid electrolyte-soaked LLTO/PAN composite fiber-based membranes were determined by linear sweep voltammetry. The measurements were carried out using cells containing liquid electrolyte-soaked LLTO/PAN composite fiber-based membranes sandwiched between stainless-steel working electrode and lithium counter electrode. The Reference 600 Potentiostat/Galvanostat/ZRA (GAMRY) was used to record the electrochemical stability windows under the scan rate of 10 mV s^{-1} and the potential range of 2.5–6.0 V at room temperature.

The interfacial resistances between liquid electrolyte-soaked LLTO/PAN composite fiber-based membranes and lithium metal electrodes were measured by monitoring the impedance of symmetrical lithium cells under open-circuit conditions. The experiments were carried out over a frequency range of 65 kHz to 0.01 Hz using the same instrument for the ionic conductivity measurement.

The electrochemical performance of lithium/LiFePO$_4$ cells containing liquid electrolyte-soaked LLTO/PAN composite fiber-based membranes was evaluated using 2032 coin cells (Hohsen Corp). Coin cells were assembled in a high-purity argon-filled glove box by sandwiching liquid electrolyte-soaked LLTO/PAN composite fiber-based membranes between lithium electrodes (0.38 mm thick, Aldrich) and LiFePO$_4$ electrodes, consisting of active material LiFePO$_4$ (80 wt.%, Hydro-Qubec), acetylene black (10 wt.%, Fisher Scientific) and polyvinylidene fluoride binder (10 wt.%, Aldrich). Charge and discharge were conducted using an Arbin automatic battery cycler in the potential window of 4.2–2.5 V at 0.2 C rate.

3. Results and discussion

3.1. LLTO structure

Fig. 1 shows the SEM image of LLTO particles. It is seen that the size of the particles ranges from tens of nm to hundreds of nm, with an average size of 200 nm. Fig. 2 shows the XRD pattern of LLTO particles. It is seen that all peaks in the obtained LLTO pattern correspond to the reflections of the perovskite structures of $Li_{0.35}La_{0.55}TiO_3$ and $Li_{0.125}La_{0.625}TiO_3$ [15,16,18–23,]. The formation of $Li_{0.125}La_{0.625}TiO_3$, which is different from the nominal composition (Li:La:Ti = 0.35:0.55:1.00) of starting materials, could be ascribed to the slight loss of lithium content during calcination at high temperature. The perovskite exhibits various crystal
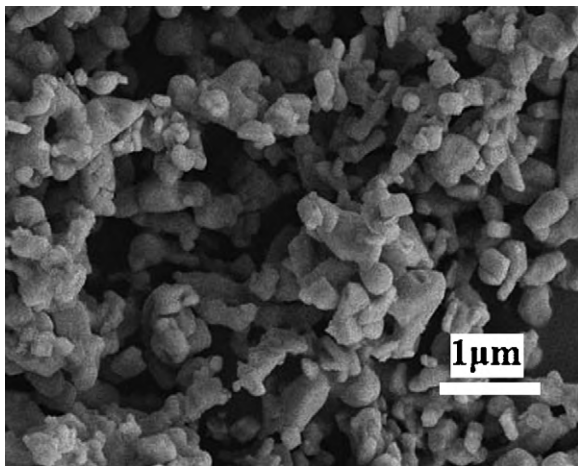
Fig. 1. SEM image of LLTO particles prepared at 900 °C for 2 h.

structures, depending on the preparation conditions (temperature, annealing ambient, etc.) and the nature of substituent.

3.2. Composite fiber morphology

Fig. 3 shows the SEM images and the diameter distributions of LLTO/PAN composite fiber-based membranes with different LLTO contents. Pure PAN fibers (0 wt.% LLTO) have smooth surface, and are relatively uniform, taut and randomly oriented, forming a spider web-like interwoven network. The average diameter of these fibers is about 250 nm. The addition of 5 wt.% LLTO leads to the formation of a small number of irregularities and uneven surface morphology, and the resultant LLTO/PAN fibers display narrower fiber diameter distribution, with an average diameter of about 230 nm. With further increase in LLTO content (e.g., 10 and 15 wt.%), the surface roughness of the electrospun LLTO/PAN fibers increases, and some LLTO particles begin to agglomerate and form clusters. In addition, the average diameters of these fibers become smaller than 200 nm. The changes in fiber diameter and diameter distribution may be attributed to the altered surface tension, electrostatic repulsion and viscoelastic force caused by the presence of lithium-ion conducting LLTO particles [24,25].
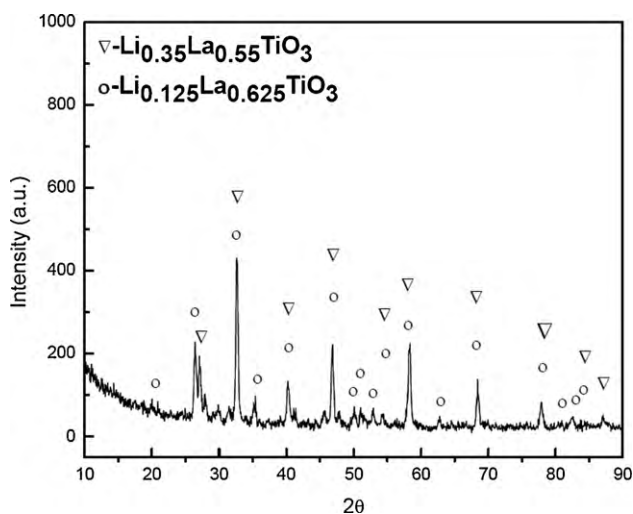

Fig. 2. XRD pattern of LLTO particles recorded at room temperature, after calcination at 900 °C for 2 h.

3.3. Liquid electrolyte uptake

Fig. 4 shows the liquid electrolyte uptakes as a function of LLTO content for LLTO/PAN composite fiber-based membranes at room temperature. The liquid electrolyte used was 1 M LiPF$_6$ in 1:1 EC/EMC. It is seen that the electrolyte uptake increases slightly with increase in LLTO content. The electrolyte uptake is dependent on the membrane morphology, e.g., fiber diameter. As shown in Fig. 3, when LLTO content increases from 0 to 5 wt.%, the average fiber decreases from around 250 to 200 nm. The decreased fiber diameter may leads to larger surface area and higher porosity [14], and hence the electrolyte uptake increases gradually from 480 to 516%.

3.4. Ionic conductivity

Fig. 5 shows the temperature dependence of the ionic conductivities of liquid electrolyte-soaked LLTO/PAN composite fiber-based membranes. For comparison, the result for liquid electrolyte-soaked PAN fiber membrane (0 wt.% LLTO) is also shown. It is seen that, for all four liquid electrolyte-soaked membranes, the ionic conductivities increase with increase in temperature. In addition, the presence of LLTO particles has influence on the conductivities of the membranes. Fig. 6 shows the conductivities as a function of LLTO content for liquid electrolyte-soaked LLTO/PAN composite fiber-based membranes. It is evident that at all temperatures, the ionic conductivities increase with increase in LLTO content. For example, the ionic conductivity of liquid electrolyte-soaked PAN fiber membrane is 8.7×10^{-4} S cm^{-1} at room temperature. The conductivity increases to 1.95×10^{-3} S cm^{-1} when the LLTO content increases to 15 wt.% LLTO at room temperature. The presence of LLTO particles decreases the fiber diameter and increases the surface area of LLTO/PAN fibers, which can help the fiber membranes entrap more liquid electrolyte, i.e., leading to increased electrolyte uptake (Fig. 4). This may be the main reason for the increased conductivities at high LLTO contents. In addition, LLTO has high bulk conductivity (10^{-3} S cm^{-1} at room temperature), which is the result of the large concentration of La-site vacancies and the high mobility of lithium by a vacancy mechanism through the wide bottleneck between the La sites [16]. Therefore, the high conductivity of LLTO may also partially contribute to the enhanced conductivities of liquid electrolyte-soaked LLTO/PAN composite fiber-based membranes.

3.5. Electrochemical stability window

Kinetic electrochemical stability window is also an important parameter in characterizing battery separators. In this study, this parameter is determined by linear sweep voltammetry on coin-type half-cells containing liquid electrolyte-soaked composite fiber-based membranes sandwiched between stainless-steel working electrode and lithium counter electrode in the potential range, where the redox reactions occur (Fig. 7). The voltage corresponding to the onset of a steady increase in the observed current density indicates the anodic stability limit of the electrolyte-soaked membrane [14,26,27].

As shown in Fig. 7, liquid electrolyte-soaked PAN fiber membrane shows an electrochemical stability window of around 5.0 V [14]. The oxidation stabilities of liquid electrolyte-soaked LLTO/PAN composite fiber-based membranes are significantly higher, with the highest stability window of 5.7 V achieved when the LLTO content is the largest (15 wt.%). Therefore, the LLTO particles act as stabilizer, and enhance the stability of liquid electrolyte-soaked fiber membranes. Such effect of ceramic particles has also been found in other composite electrolyte systems [14]. The high electrochemical stability of liquid
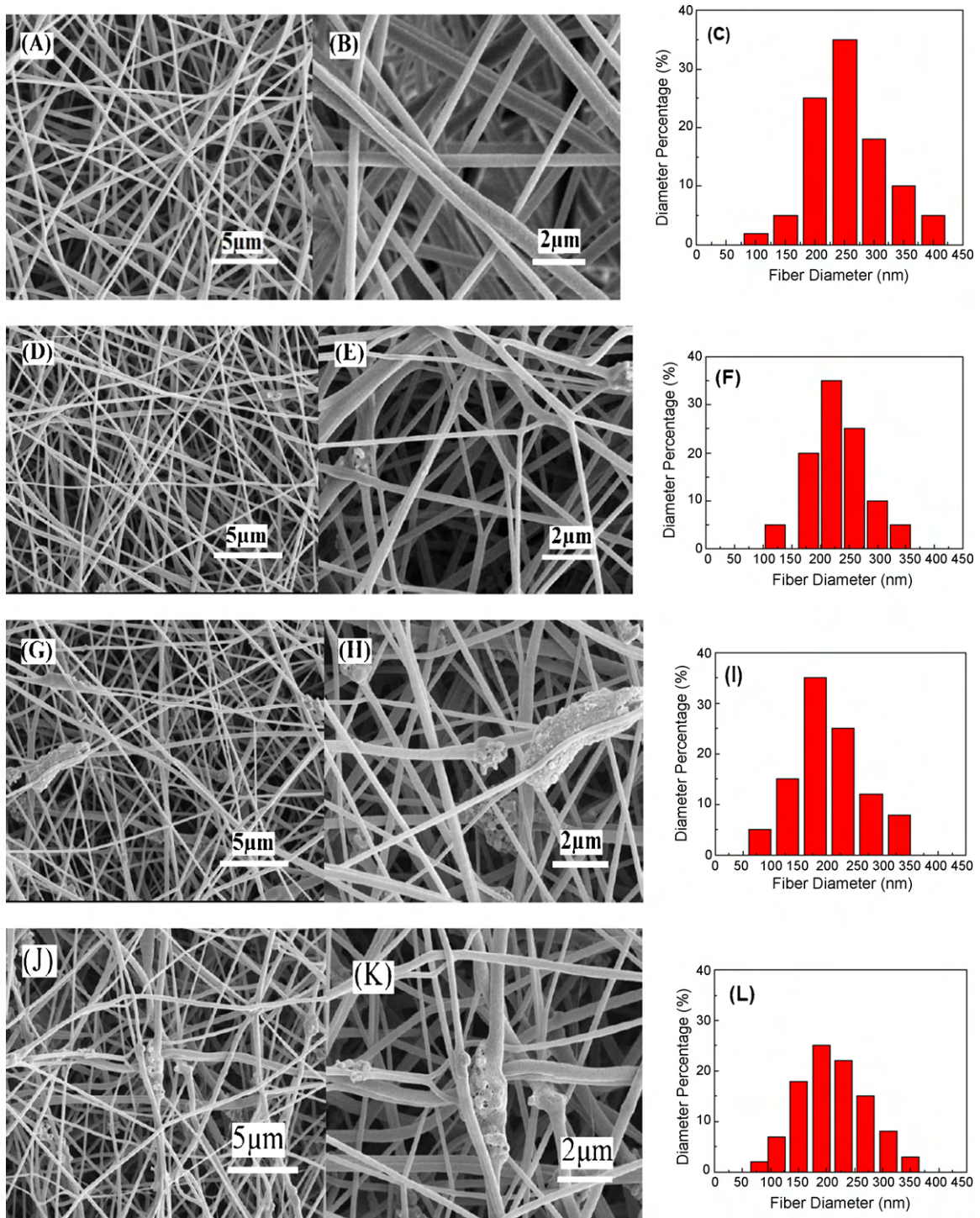
Fig. 3. SEM images and diameter distributions of LLTO/PAN composite fiber-based membranes with different LLTO contents: (A–C) 0 wt.%, (D–F) 5 wt.%, (G–I) 10 wt.%, and (J–L) 15 wt.%.

electrolyte-soaked LLTO/PAN composite fiber-based membranes should render them potentially compatible with most high-voltage cathode materials used for rechargeable lithium-ion batteries [14].

3.6. Interfacial resistance

The electrochemical impedance spectra of Li/liquid electrolyte-soaked membrane/Li cells are shown in Fig. 8. The diameter of the intermediate-frequency semicircle indicates the electrode–electrolyte interfacial resistance R_i [14]. As shown in Fig. 8, the order of R_i values is: 15 wt.% LLTO/PAN composite fiber-based membrane < 12 wt.% LLTO/PAN composite fiber-based membrane < 10 wt.% LLTO/PAN composite fiber-based membrane < 5 wt.% LLTO/PAN composite fiber-based membrane < 0 wt.% LLTO/PAN fiber membrane. The addition of LLTO particles can help trap impurities from the liquid electrolyte, which may lead to smaller interfacial resistance at high LLTO contents. Similar phenomenon has been found in ceramic particle-filled polymer and gel electrolytes [28,29].
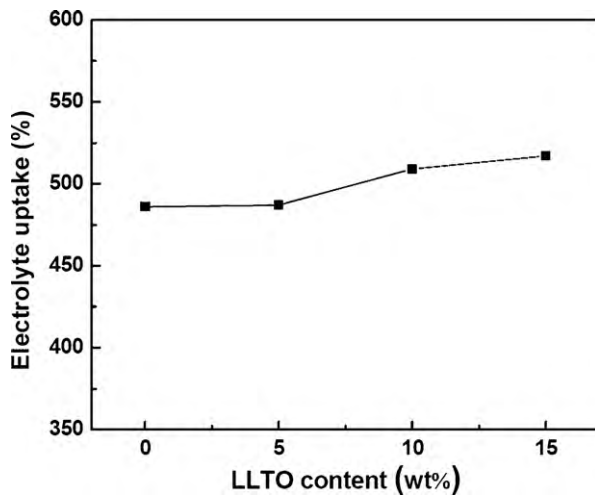
Fig. 4. Electrolyte uptakes of electrospun LLTO/PAN composite fiber-based membranes.
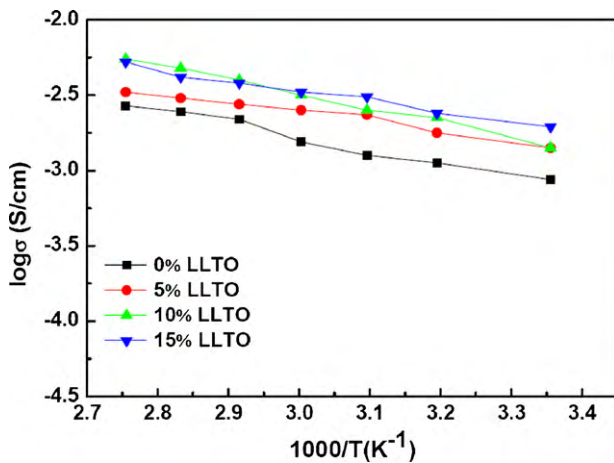

Fig. 5. Ionic conductivities of liquid electrolyte-soaked electrospun LLTO/PAN composite fiber-based membranes with different LLTO contents.
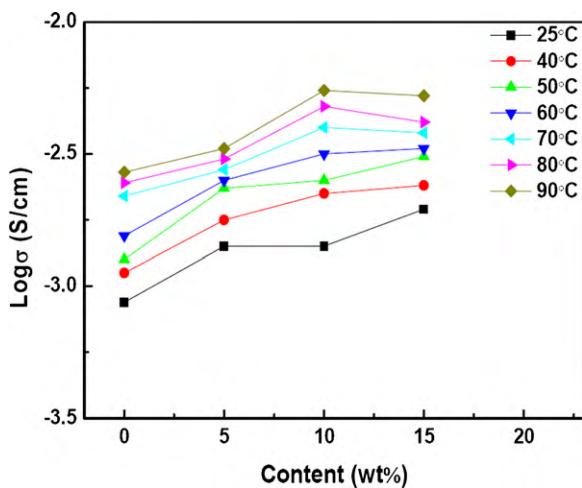

Fig. 6. Ionic conductivities as a function of LLTO content for liquid electrolyte-soaked electrospun LLTO/PAN composite fiber-based membranes at various temperatures.
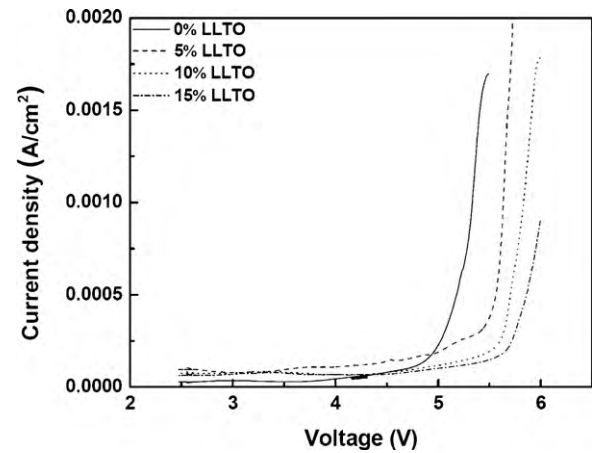

Fig. 7. Electrochemical stability windows of liquid electrolyte-soaked electrospun LLTO/PAN composite fiber-based membranes with different LLTO contents.

3.7. Battery performance

In order to further examine the feasibility of using PAN and LLTO/PAN composite fiber-based membranes as separators in rechargeable LIBs, coin-type half-cells were fabricated with LiFePO$_4$ as the cathode and lithium metal as the counter electrode. For comparison, the cells using commercial Celgard 2400 separator were also prepared. The first-cycle charge and discharge curves at room temperature are shown in Fig. 9. All the curves show stable charge and discharge platforms, and the initial specific discharge capacities of all cells are between 148 and 162 mAh g^{-1}. However, cells using liquid electrolyte-soaked PAN fiber membrane have higher charge and discharge capacities than those using electrolyte-soaked Celgard 2400. Furthermore, the addition of LLTO particles in composite fiber membrane separator further increases the capacities.

Fig. 10 shows the discharge capacity versus cycle number for the cells subjected to 50 cycles at room temperature. At the 50th cycle, cells using liquid electrolyte-soaked 10 wt.% LLTO/PAN composite fiber-based membrane have the highest discharge capacity of 156 mAh g^{-1}, which is 91.7% of the theoretical capacity of LiFePO$_4$ (170 mAh g^{-1}). That result confirms the excellent efficiency of the liquid electrolyte-soaked LLTO/PAN composite fiber-based membranes to conduct lithium ions between electrodes during cycling process. Therefore, liquid electrolyte-soaked LLTO/PAN compos-
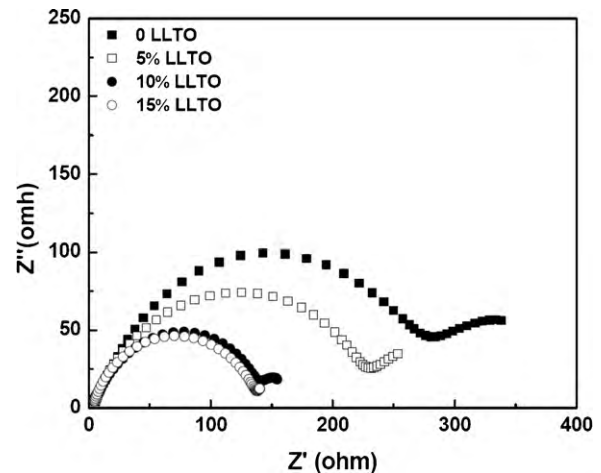

Fig. 8. Electrochemical impedance spectra of liquid electrolyte-soaked LLTO/PAN composite fiber-based membranes with different LLTO contents.
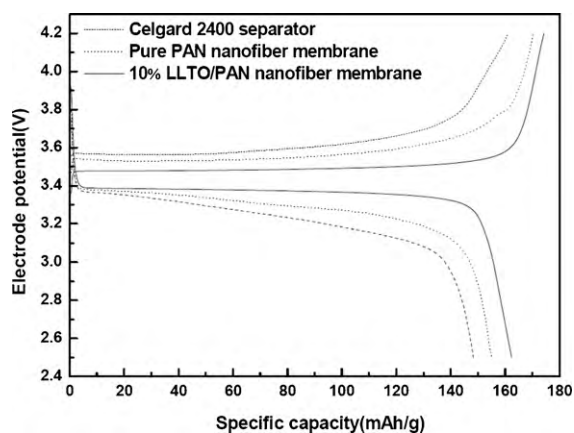
Fig. 9. First-cycle charge and discharge curves of Li/LiFePO$_4$ cells containing liquid electrolyte-soaked Celgard 2400 separator, pure PAN fiber-based membrane and LLTO/PAN composite fiber-based membrane at 0.2 C rate.

Fig. 10. Cycle performance of Li/LiFePO$_4$ cells containing liquid electrolyte-soaked Celgard 2400 separator, PAN fiber-based membrane and LLTO/PAN composite fiber-based membrane at 0.2 C rate.
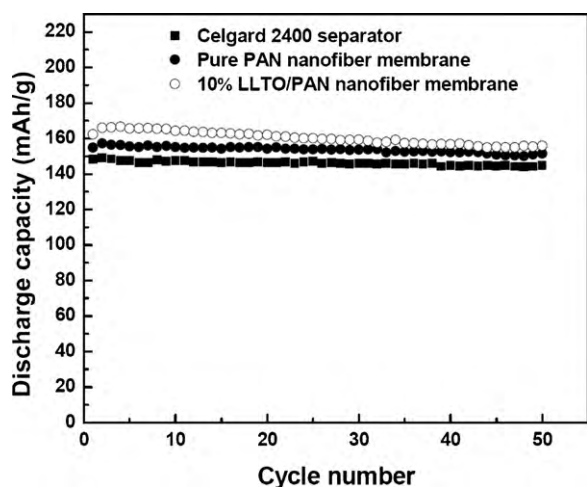
ite fiber-based membranes are promising separator candidate for rechargeable LIBs.

4. Conclusions

The electrospinning technology was used to fabricate LLTO/PAN composite fiber-based membranes for rechargeable LIBs. It is found that with increase in LLTO content, the average fiber diameter of LLTO/PAN fibers decreases slightly. As a result, after the addition of 15 wt.% LLTO particles, the liquid electrolyte-soaked composite membrane shows a high ionic conductivity of 1.95×10^{-3} S cm^{-1} at room temperature. The liquid electrolyte-soaked LLTO/PAN composite fiber-based membranes exhibit lower interfacial resistance, higher electrolyte uptake, and higher electrochemical stability window than liquid electrolyte-soaked pure PAN fiber membrane. Liquid electrolyte-soaked LLTO/PAN composite fiber-based membranes also show good compatibility with lithium electrode. In addition, cells containing liquid electrolyte-soaked LLTO/PAN composite fiber-based electrospun membranes have an initial discharge capacity of 166 mAh g^{-1} and a stable cycle performance at 0.2 C rate.

References

[1] M. Armand, J.-M. Tarascon, Nature 451 (2008) 652–657.
[2] A. Manthiram, A.V. Murugan, A. Sarkar, T. Muraliganth, Energy Environ. Sci. 1 (2008) 621–638.
[3] Y.G. Guo, J.S. Hu, L.J. Wan, Adv. Mater. 20 (2008) 2878–2887.
[4] M.G. Kim, J. Cho, Adv. Funct. Mater. 19 (2009) 1497–1514.
[5] J. Saunier, F. Alloin, J.Y. Sanchez, G. Caillon, J. Power Sources 119–121 (2003) 454–459.
[6] Y.M. Lee, J.W. Kim, N.S. Choi, J.A. Lee, W.H. Seol, J.K. Park, J. Power Sources 139 (2005) 235–241.
[7] F.G.B. Ooms, E.M. Kelder, J. Schoonman, N. Gerrits, J. Smedinga, G. Callis, J. Power Sources 97–98 (2001) 598–601.
[8] T.-H. Cho, M. Tanaka, H. Onishi, Y. Kondo, T. Nakamura, H. Yamazaki, S. Tanase, T. Sakai, J. Power Sources 181 (2008) 155–160.
[9] P.K. Arora, Z.M. Zhang, Chem. Rev. 104 (2004) 4419–4462.
[10] S.S. Zhang, J. Power Sources 164 (2007) 351–364.
[11] C.R. Yang, Z.D. Jia, Z.C. Guan, L.M. Wang, J. Power Sources 189 (2009) 716–720.
[12] S.-S. Choi, Y.S. Lee, C.W. Joob, S.G. Lee, J.K. Park, K.-S. Han, Electrochim. Acta 50 (2004) 339–343.
[13] D. Bansal, B. Meyer, M. Salomon, J. Power Sources 178 (2008) 848–851.
[14] H.R. Jung, D.H. Ju, W.J. Lee, X.W. Zhang, R. Kotek, Electrochim. Acta 54 (2009) 3630–3637.
[15] M. Vijayakumar, Y. Inaguma, W. Mashiko, M.P. Crosnier-Lopez, C. Bohnke, Chem. Mater. 16 (2004) 2719–2724.
[16] S. Stramare, V. Thangadurai, W. Weppner, Chem. Mater. 15 (2003) 3974–3990.
[17] G.Y. Adachi, N. Imanaka, S.J. Tamura, Chem. Rev. 102 (2002) 2405–2429.
[18] K. Dokko, N. Akutagawa, Y. Isshiki, K. Hoshina, K. Kanamura, Solid State Ionics 176 (2005) 2345–2348.
[19] M. Hara, H. Nakano, K. Dokko, S. Okuda, A. Kaeriyama, K. Kanamura, J. Power Sources 189 (2009) 485–489.
[20] Y. Inaguma, C. Liquan, M. Itoh, T. Nakamura, T. Ichida, H. Ikuta, M. Wakihara, Solid State Commun. 86 (1993) 689.
[21] A. Belous, O. Yanchevskiy, O. V'yunov, Chem. Mater. 16 (2004) 407–417.
[22] A. Varez, Y. Inaguma, M.T. Fernández-Diaz, J.A. Alonso, J. Sanz, Chem. Mater. 15 (2003) 4637–4641.
[23] M. Catti, J. Phys.: Conf. Ser. 117 (2008) 012008.
[24] L. Ji, A.J. Medford, X.W. Zhang, Polymer 50 (2009) 605–612.
[25] L. Ji, A.J. Medford, X.W. Zhang, J. Mater. Chem. 19 (2009) 5593–5601.
[26] X. Li, G. Cheruvally, J.-K. Kim, J.-W. Choi, J.-H. Ahn, K.-W. Kim, H.-J. Ahn, J. Power Sources 167 (2007) 491–498.
[27] G. Cheruvally, J.K. Kim, J.-W. Choi, J.H. Ahna, Y.J. Shin, J. Manuel, P. Raghavan, K.W. Kim, H.J. Ahn, D.S. Choi, C.E. Song, J. Power Sources 172 (2007) 863–869.
[28] X.W. Zhang, C.S. Wang, A.J. Appleby, F.E. Little, J. Power Sources 112 (2002) 209–215.
[29] X.W. Zhang, Y. Li, S.A. Kban, P.S. Fedkiw, J. Electrochem. Soc. 151 (2004) A1257–A1263.